ARTICLE TYPE

A New Approach for the Fabrication of Microscale Lipid Bilayers at Glass Pipets: Application to Quantitative Passive Permeation Visualization

Katherine E. Meadows[a,b] Binoy Paulose Nadappuram[a] and Patrick R. Unwin*[a]

A new method of planar bilayer lipid membrane (BLM) formation is presented that allows stable, solvent-free lipid bilayers exhibiting high seal resistances to be formed rapidly, easily and reproducibly. Using these bilayers the passive permeation of a series of carboxylic acids is investigated, to determine quantitatively the trend in permeability with lipophilicity of the acid. BLMs are formed at the tip openings of pulled theta pipets, and the rate of permeation of each carboxylic acid across the bilayer, from within the pipet into the bulk solution is determined. This is achieved through spatially-resolved measurements of the pH change that occurs upon the permeation of the weak acid, visualized using a pH-sensitive fluorophore with a confocal laser scanning microscope. The extracted fluorescence profiles are matched to finite element method (FEM) simulations, to allow the associated permeation coefficient for each weak acid to be determined with high accuracy, since this is the only adjustable parameter used to fit the experimental data. For bilayers formed in this way, the weak acids show increasing permeability with lipophilicity. Furthermore, the arrangement allows the effect of a trans-membrane electric field on permeation to be explored. For both propanoic and hexanoic acid it is found that an applied electric field enhances molecular transport, which is attributed to the formation of pores within the membrane.

Introduction

Planar lipid bilayers have been used extensively as model cell membranes for the study of passive permeation processes for many years.[1-8] Passive permeation across the cell membrane is of particular interest since most drug compounds are transported via this mechanism, and, as such, planar lipid bilayers are used in both high throughput drug screening[9-11] and more detailed studies to identify trends in permeation rates between molecules,[2, 3, 5, 6] in addition to studies of charge transfer across the membrane.[12, 13] Permeation coefficients of small molecules have commonly been analyzed using Overton's rule,[14] which considers the permeation coefficient, *P*, of a molecule transported across a membrane between two aqueous solutions to be proportional to the product of the partition coefficient, *K*, and diffusion coefficient, *D*, of the molecule in the membrane.[15] There has, however, been some debate as to whether this simplistic view of the permeation process is sufficient to describe the permeation of all small molecules, since it does not take into account the amphipathic nature of the phospholipids in a lipid bilayer. Whilst the majority of studies show a positive correlation between lipophilicity and permeation rate, the relationship is often not linear[4, 16] and there is considerable variation in the *P* values reported for the same molecules.[2, 3, 5, 7] Some studies have observed contrasting trends for the same series of molecules, suggesting that permeation processes may be more complex.[1, 17] However, several of the existing experimental techniques are limited in the range of permeation coefficients that may be measured accurately. Moreover, the method of bilayer production may affect the properties of the membrane formed, which may in turn influence the permeation process.[18]

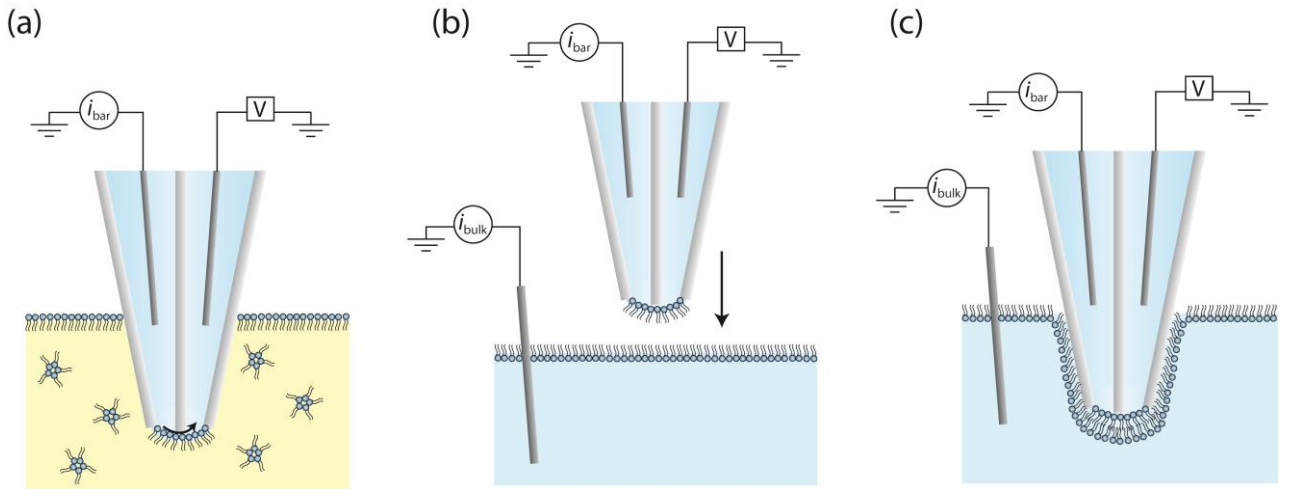

Figure 1. Schematic illustration (not to scale) of the bilayer formation process. A theta pipet (outer walls silanized) is lowered into a lipid solution (in chloroform) while applying a small potential between the two QRCEs to ensure the meniscus is well-formed (a). The pipet is held in the solution for approximately one minute before it is retracted, and the cell and solution replaced with an aqueous electrolyte. A small volume of lipid solution (in chloroform) is dropped onto the aqueous electrolyte and the volatile organic solvent allowed to evaporate forming a lipid monolayer (b). The pipet is then slowly lowered until the two monolayers make contact and a bilayer is formed (c).

One of the most widely used procedures, the painting method,[19] produces lipid bilayers which contain residual solvent molecules in the interior of the bilayer, raising questions about the integrity and reliability of such model membranes.[20] Other methods produce bilayers with little or no residual solvent,[21] but these may have comparatively short lifetimes.[22] Improvements in BLM stability have been achieved through the use of gel-phase materials which have produced bilayers that are extremely durable.[23-27] However, due to the slow diffusion of analytes through the gel, the temporal responses are very slow.[28] The use of small apertures, over which a bilayer is suspended, can also improve electrical and mechanical stability.[29, 30]

Liposomes have also been used, which do not contain any residual solvent molecules in the interior of the membrane, and are typically stable for considerably longer periods than planar lipid bilayers.[31] However, since the interior of the liposome is inaccessible for sampling, measurement of permeation rates can be difficult. Recently confocal laser scanning microscopy (CLSM) has been employed to give increased resolution of the permeation of molecules into a single liposome.[32] Using this technique, it is possible to study not only fluorescent permeants but also weak acids, by means of a pH-sensitive fluorophore, enabling visualization of local pH changes as the molecule permeates either into a liposome[16] or, as originally reported, across a planar lipid bilayer.[1]

Here, we report on the use of dual-barrel theta capillaries for the formation of stable, solvent-free, suspended BLMs. This could be viewed as a modification of the tip-dip method reported previously,[22, 33, 34] but herein, the monolayer is formed directly from a lipid solution rather than by moving the pipet out and into a solution that contains a lipid monolayer at the air-water interface. Long lasting bilayers that are formed simply, quickly and reproducibly with high success rate (nearly 100%) (exhibit resistances up to 600 GΩ). Using this system, we determine the permeation coefficients of a series of aliphatic carboxylic acids as they passively permeate across a bilayer. By using CLSM with a pH-sensitive fluorophore,[1, 16] the movement of these molecules can be tracked by monitoring the local pH changes around the end of the pipet. Combining this with FEM modeling, permeation coefficients for the series of acids can be extracted to determine the effect of permeant lipophilicity on permeability, using just one adjustable parameter (permeation coefficient) to model the data Significantly, the trends observed are in quantitative agreement with measurements on solvent-free liposomes, confirming the validity of the technique. An attractive aspect of the methodology is that the effect of a potential field on the permeation rate of molecules can also be investigated, simply by positioning quasi-reference counter electrodes (QRCEs) on each side of the bilayer. Experimental investigations of the electric field effect on membrane transport are thus reported.

Principles

The simple method of BLM fabrication presented herein enables the rapid formation of solvent-free, suspended bilayers with exceptional electrical properties. To form these bilayers, a pulled theta glass pipet is filled with electrolyte solution and a QRCE (Ag/AgCl wire) is inserted into each barrel. A small potential (typically 100 mV) is applied between the two to ensure there is a well-formed meniscus at the end of the pipet before it is immersed into the lipid solution (1 mg/ml lipid in chloroform) (Figure 1 (a)).

This concentration is sufficiently high that a monolayer assembles at the oil/water interface. Upon immersion, the resistance between the QRCEs in the pipet barrels increases from ~3-5 MΩ to ~2-10 GΩ. The pipet is held in the lipid solution for approximately one minute to allow the monolayer to assemble, after which, it is removed, leaving the monolayer intact on the meniscus of the pipet and allowing any residual volatile solvent molecules to easily evaporate (Figure 1(b)). The pipet is then positioned above an electrolyte solution, onto the surface of which a small amount of lipid solution (10 µl) is dropped,

forming a monolayer at the air/water interface. The volume of lipid solution required to ensure full monolayer coverage was determined by recording pressure/area isotherms for 1,2-dipalmitoyl-*sn*-glycero-3-phosphocholine (DPPC) monolayers (used for the majority of experiments) using a Langmuir trough (see section S2 in the Supporting Information), and corresponded to a surface pressure of ca. 50 mN m^{-1}, similar to the pressure of cell membranes.[35]

The pipet is slowly lowered until the two monolayers make contact and a bilayer is formed (Figure 1 (c)). Once formed, the current between one of the QRCEs in the pipet and a third QRCE in the bulk solution (i_{bulk}) is monitored as the potential is scanned linearly to determine the resistance of the bilayer from the slope of the current-voltage curves produced.

Further, to validate the formation of a bilayer on the tip, gramicidin ion-channel incorporated bilayers were formed by the same procedure but using a 1mg/ml lipid solution containing 0.5% (w/w) gramicidin. The ion current between the QRCEs in the pipet and bulk solution was monitored while the potential was swept linearly to determine any change in bilayer resistance due to the incorporation of gramicidin ion-channels into the bilayer.

For the measurement of permeation coefficients, the pipets are filled with the weak acid solution which is pH corrected to ensure the protonated form of the weak acid is the dominant species. Since charged species cannot permeate the bilayer to any detectable extent, it is important to ensure the carboxylic acids are in the neutral form.[36] The bulk solution, into which the molecules permeate, contains the pH-sensitive fluorophore fluorescein, and is adjusted to pH 8 so that any permeating weak acid molecules tend to dissociate, changing the pH locally. This pH change can be visualized using the confocal laser scanning microscope and the resulting fluorescence profiles analyzed with FEM simulations to elucidate permeation coefficients, as described herein.

Theory and Simulations

Using FEM modeling, the steady-state fluorescence profiles that arise due to the permeating weak acid can be simulated as a function of permeation coefficient, which is the only adjustable parameter when matching simulations to experiment. For each weak acid (HX) studied, the following solution process was considered:

$$HX \leftrightarrow X^- + H^+ \qquad (0)$$

where X^- is the conjugate anion of the weak acid, the concentration of which is dependent on the local pH and pK_a of the weak acid. The bulk electrolyte solution was weakly buffered with 50 μM HEPES and thus the three protonation states of this buffer (neutral, negatively charged and doubly negatively charged) were also included. The protonation state of fluorescein has been shown to have no significant effect at the concentrations used here and was therefore ignored in the calculations.[1]

The very fast kinetics of the protonation processes compared to the experimental timescale mean that they could be considered as equilibria controlled by the local pH. To ensure the equilibria were handled correctly, the pKa values for the weak acid and buffer were corrected for ionic activity using the Davies equation.[37]

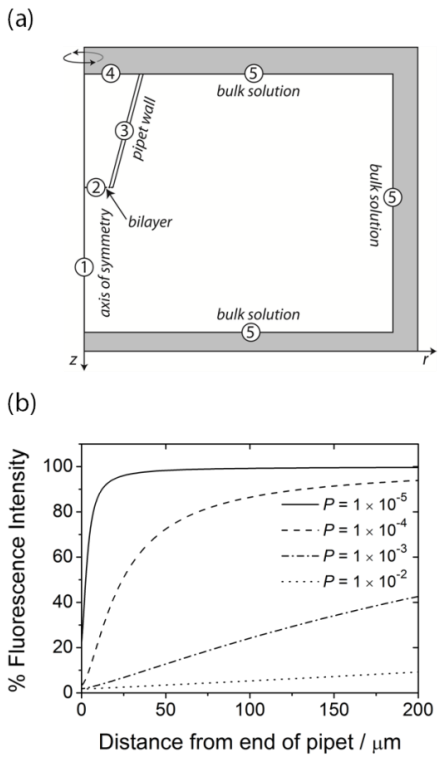

Figure 2. (a) Axi-symmetric cylindrical simulation domain for permeation coefficient determination. The pipet geometry is determined from optical microscopy and a range of permeation coefficients for the diffusion of the weak acid across the bilayer are simulated. (b) Series of simulated fluorescence profiles at different P values (units cm s-1) for the permeation of 100 mM propanoic acid (see text for other parameters).

For each species, *i*, in the simulation (H^+, X^-, HX, HEPES, $HEPES^-$, $HEPES^{2-}$), a time-independent solution to the following reaction-diffusion equation was sought:

$$D_i\left(\frac{\partial^2 c_i}{dr^2}+\frac{1}{r}\frac{\partial c_i}{\partial r}+\frac{\partial^2 c_i}{\partial z^2}\right)+R_i=0 \qquad (0)$$

where c_i and D_i are the concentration and diffusion coefficient of species, *i*, respectively, *r* and *z* are the radial and normal coordinates with respect to the center of the pipet (axi-symmetric cylindrical geometry), and R_i is the rate of production of species *i* in the domain (shown in Figure 2(a)).

The finite element method was used to determine the steady-state concentration of each of the species by solving equation 2 subject to the boundary conditions of the system, which are summarized in Table 1. Here $N_{bilayer}$ describes the flux of the neutral weak acid across the bilayer (with c_i^{out} and c_i^{in}, the concentration of the species on either side of the bilayer; c_i^{out} is the concentration outside the pipet, in the bulk solution, and c_i^{in} is the concentration inside the pipet). The initial bulk concentrations of each of the species, *i*, inside and outside of the pipet are denoted c_i^{in*} and c_i^{out*}.

Table 1: Summary of the boundary conditions used for the simulation of the permeation of a weak acid across a bilayer

Label in Figure 2	Boundary	Equation
1	Axis of symmetry	$0 = \nabla c_i . \underline{n}$
2	Bilayer	$N_{bilayer} = P\left(c_{HX}^{out} - c_{HX}^{in}\right)$ $0 = \nabla c_j . \underline{n}$ j = all other species
3	Pipet wall	$0 = \nabla c_i . \underline{n}$
4	Top of pipet	$c_i^{in} = c_i^{in*}$
5	Bulk solution	$c_i^{out} = c_i^{out*}$

The resulting steady-state profiles for H^+ were converted to pH and subsequently to fluorescence intensity (I) using the empirical relation determined previously in our group for the pH dependency of fluorescein fluorescence intensity, which was found to apply under these conditions:[1]

$$I = 1 - \frac{0.983}{1 + e^{-3.36(6.18 - \mathrm{pH})}} \qquad (0)$$

A series of simulation profiles are shown for a typical acid (propanoic acid) which visibly demonstrates that this methodology is sensitive to permeation rates over 4 orders of magnitude (Figure 2(b)). Moreover, it is easily tuneable to a particular region by altering the experimental conditions: the pipet geometry, the pH of the internal and external solutions, and the buffer concentrations can all be varied.

Experimental

4.1 Reagents

Aqueous solutions were prepared with 18.2 MΩ cm (25 °C) Milli-Q water (Millipore Corp.). Carboxylic acid solutions were prepared using 0.1 M KCl (Sigma-Aldrich), 5 µM of the sodium salt of fluorescein (Sigma-Aldrich) and a designated concentration of either sodium acetate, sodium propionate, sodium butyrate or sodium hexanoate (Sigma-Aldrich). The pH of these solutions was adjusted to ~4.2 with 18 M HCl (Fisher Scientific) to ensure the protonated form of the weak acid was the dominant species (pK_a of each weak acid defined in the Supporting Information, Table S1). A buffered electrolyte solution containing 0.1 M KCl, 50 µM HEPES (Fluka) and 5 µM of the sodium salt of fluorescein was also prepared and adjusted to pH 8 using NaOH (Fisher Scientific). Due to the relatively high pH in the bulk solution, the speciation of HEPES was such that the concentration of the neutral molecule was less than 0.1 nM and so did not need to be considered as a permeating species. For bilayer formation, DPPC or soy phosphatidylcholine (95%) (Avanti Polar Lipids) were dissolved in chloroform (BDH) to a concentration of 1 mg/ml.

4.2 Bilayer Formation and Recording Setup

Borosilicate glass theta capillaries (1.5 mm outer diameter, Harvard Apparatus Ltd) were pulled using a laser puller (P-2000, Sutter Instruments, USA) to produce pipets with tapered tip openings 5-10 µm in diameter (measured by optical microscopy). The two pipet barrels were filled with the weak acid solution to approximately half way using a MicroFil (World Precision Instruments, Inc.). The remaining details are given in Section 2. Two purpose-built high sensitivity current to voltage converters were used to simultaneously record the currents between the barrels (i_{bar}) and across the bilayer, between the barrel and bulk solution (i_{bulk}); see schematic in Figure 1(c).

4.3 Confocal Laser Scanning Microscopy

CLSM experiments were performed using a Leica TCS SP5 X confocal fluorescence system on a Leica DMI6000 inverted microscope. An Ar laser at 488 nm was used to excite the fluorescein in solution and the resulting emission was collected between 500 and 540 nm. Samples were mounted on an aluminum sample holder (fabricated in house) and the entire assembly was housed in a Faraday cage mounted on the CLSM stage. For visualization of weak acid permeation, the line scan frequency was 1400 Hz. After bilayer formation, the system was allowed to equilibrate for ~30 s before a series of images were collected in the plane parallel to the bilayer at 1 µm intervals in the z-direction, to produce a 3D fluorescence image, related to the weak acid diffusion profile (see above).

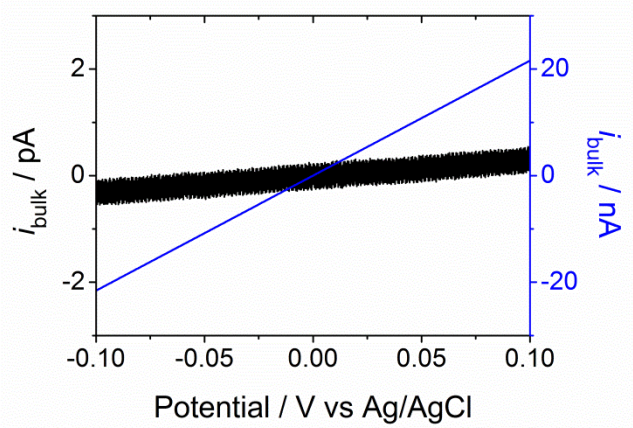

Figure 3. Typical current-voltage curves for an 8 µm diameter pipet containing 0.1 M KCl and 5 µM fluorescein in the bulk solution (0.1 M KCl, 50 µM HEPES and 5 µM fluorescein) before (blue line, right y-ordinate) and after (black line, left y-ordinate) bilayer formation. The open pipet and bilayer seal resistances are 4.6 MΩ and 330 GΩ, respectively.

4.4 Data Analysis

CLSM images were analyzed with MATLAB 2010a (Mathworks Inc., Cambridge, UK) to produce fluorescence profiles normal to the end of the pipet. A polynomial fit was applied to the data to reduce the experimental noise whilst preserving the shape of the profile (see Supporting Information, Section S3 for details). These polynomial fits were then matched to simulated profiles produced using COMSOL Multiphysics 4.2a (COMSOL AB, Sweden) to extract a permeation coefficient. For each pipet, the COMSOL model was parameterized from the experimental geometry and typically 135,000 mesh elements were used, with the greatest resolution around the end of the pipet. Measurements

were made on 2-3 bilayers for each acid and the errors shown on the resulting permeation coefficient are the standard deviation.

Results and Discussion

5.1 Bilayer characterization

After the formation of a lipid bilayer, suspended across the orifice of the pipet, the seal resistance was measured by recording current-voltage curves, with the potential applied between the QRCEs on each side of the bilayer. The resistance varied over a fairly narrow range from ~100 GΩ to ~600 GΩ, with an average value of 260 ± 140 GΩ based on ~15 independent measurements on different bilayers. These values are comparable to those previously reported in the literature for bilayers formed on similar sized apertures.[29, 38, 39] Figure 3 shows typical *i*-V curves between a QRCE in the pipet and one in the bulk solution, before and after bilayer formation, with a typical increase in resistance of 5 orders of magnitude. For these measurements, as shown in Figure 1(c), the potential of one of the QRCEs in the pipet was swept (with respect to ground) whilst the current was recorded at the QRCE in the bulk solution (on the other side of the bilayer) held at ground. In order to verify the formation of a bilayer on the pipet tip, *i-V* curves were recorded between the QRCEs in the pipet and the bulk solution for a gramicidin incorporated bilayer membrane (Supporting Information section S1). In a bilayer membrane, gramicidin acts as an ion-channel allowing transport of monovalent cations (K^+ in this case), hence decreasing the bilayer membrane resistance. The membrane resistance was found to decrease from ~150 GΩ to ~13 GΩ after the incorporation of gramicidin into the bilayer, which is consistent with decrease in membrane resistances previously reported for supported bilayers confirming the assembly of a bilayer membrane at the pipet tip.[40]

These bilayers offer several advantages, most notably a negligible amount of residual solvent molecules through the use of a highly volatile carrier solvent. The bilayers produced were often stable for several hours and over a potential range from -1 to +1 V. The absence of residual solvent molecules is particularly advantageous for this study, since the passive permeation of small molecules greatly depends on the structure of the bilayer and any organic residues could affect the rate of transport, as highlighted in Section 1.

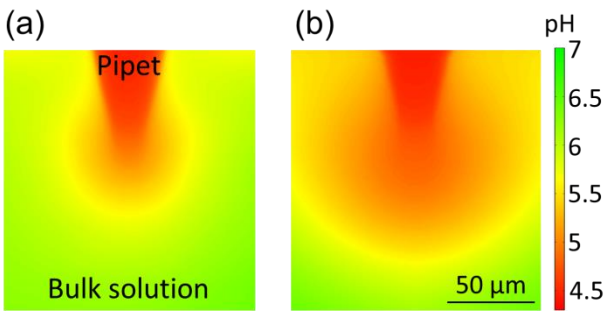

Figure 4. CLSM fluorescence intensity images showing the permeation of (a) 10 mM butanoic acid and (b) 10 mM hexanoic acid across DPPC bilayers formed on 8 µm tip diameter pipets.

5.2 Visualization of Weak Acid Transport

The microscale bilayer system, in which a suspended bilayer is formed at the tip of a tapered pipet, is advantageous compared to many existing permeation systems, since very high mass transport rates can be achieved at tapered micropipets and nanopipets in quiescent solution (without any need of stirring).[41-45] In contrast, in many previous studies permeation coefficients have typically been determined by measuring the flux of a permeant between two adjacent stirred chambers separated by a bilayer.[8] Stirring increases the rate of mass transport of the permeant to the bilayer, however, there is an unstirred region where the rate of transport is dominated by diffusion. In this unstirred layer (USL), which is often difficult to define precisely, a diffusive gradient exists between the bulk concentration of the permeant and the concentration at the bilayer interface.[46] This layer can extend for several hundred microns on either side of the bilayer and cause significant resistance to the rates of permeation that can be measured, since the rate at which a molecule crosses the USL is generally much slower than the rate of permeation across the bilayer itself.[1, 47] Failure to correct for the USL can lead to large errors in the calculation of permeation coefficients and this appears to be one factor in explaining the variation in reported permeation coefficients for the same molecules.[3, 48] The method herein of using local pH changes to detect the rate of permeation eliminates any USL problems, since the permeant is delivered directly to the bilayer, and the resulting fluorescence profile is generated in seconds unlike conventional proton titration, bulk pH or tracer molecule studies which can take several hours.[2, 5]

Figure 4 shows example pH profiles for the permeation of 10 mM butanoic and hexanoic acid across DPPC bilayers formed on pipets with 8 µm diameter tip openings. It can clearly be seen that hexanoic acid produces a significantly larger decrease in pH on the trans (bulk solution facing) side of the membrane than butanoic acid, and, since the concentration of the permeant and size of the pipet are consistent, and the pKa values of the acids is similar (Supporting Information, Table S1), the permeation coefficient must be higher in the hexanoic acid case. In fact, when the fluorescence profiles for the other acids at the same concentration are compared, there is a clear correlation between the permeation rate and acyl tail

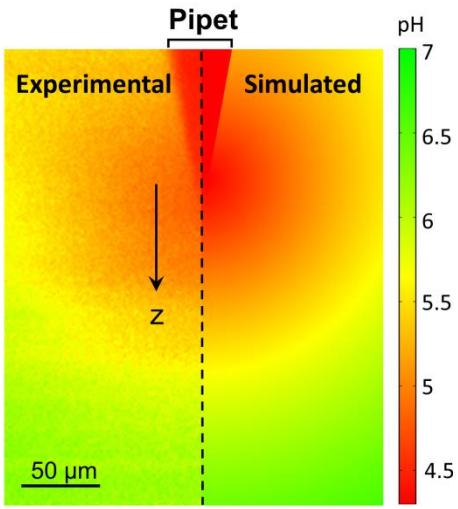

Figure 5. Experimental (left) and simulated (right) pH profile for the permeation of 100 mM propanoic acid across a DPPC bilayer located at the end of a pipet. A permeation coefficient of 7.0×10^{-4} cm s^{-1} was the only adjustable parameter used to fit the experimental data.

length, indicating that permeability increases with lipophilicity (*vide infra*).

5.3 Quantitative Determination of Permeation Coefficients

To identify the permeation coefficient, *P*, for each weak acid, a series of simulated fluorescence profiles was produced from the FEM model to allow the best match to the experimental profile to be determined (see Section 3 and Supporting Information, Section S3). *P* values were also chosen to fit the upper and lower bounds of two independent profiles from bilayers formed at different pipets. In Figure 5 we show a typical experimental profile for the permeation of 100 mM propanoic acid matched to the simulated data, using a permeation coefficient of 7.0×10^{-4} cm s^{-1} as the only adjustable parameter. Excellent agreement between experiment and simulation is evident.

To analyze data, pH profiles in the *z*-direction, normal to the membrane, extending into the bulk solution were examined. .Figure 6 shows the experimental profiles for each of the acids, which fit the simulated profiles well over the length scale shown, 25 -150 µm from the end of the pipet. Further into the solution, the effects of natural convection will influence the transport process,[49] providing an upper limit on the range of the profiles considered. Note that, as discussed in Section S4, there are some optical effects due to the finite magnification of the CLSM system, and so to reduce these, data within 25 µm of the pipet on the trans side of the membrane were not analyzed.

As expected from visual inspection of the CLSM images, the permeation coefficients of each of the weak acids were found to increase monotonically with acyl tail length and water/octanol partition coefficient, *K*. The relationship of permeation coefficient to acyl tail length is shown quantitatively in Figure 7 (a) for bilayers formed from both DPPC and soy PC. For propanoic and butanoic acid, permeation coefficients are rather

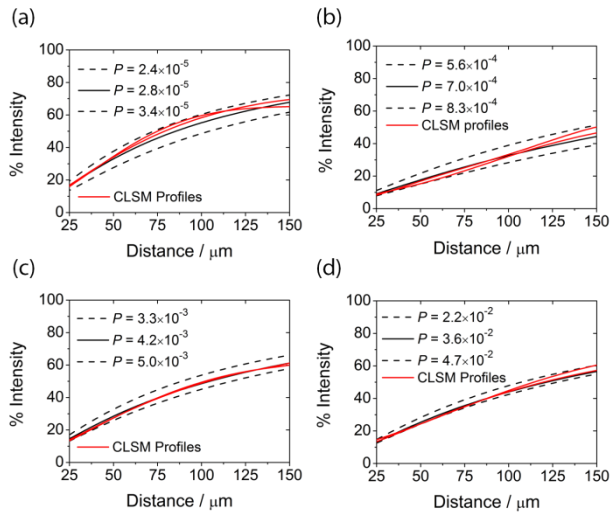

Figure 6. Experimental and corresponding simulated fluorescence-distance plot for (a) 100 mM acetic acid, (b) 100 mM propanoic acid, (c) 10 mM butanoic acid and (d) 10 mM hexanoic acid. The permeation coefficients corresponding to the upper and lower bounds and best fit of the CLSM data are shown (units cm s^{-1}).

similar for both types of bilayer. However, for weakly permeating acetic acid, it is evident that the bilayer type has a significant impact on transport rates, with much faster transport (by nearly two orders of magnitude) seen for soy PC compared to DPPC. This is because a bilayer formed from saturated lipids such as DPPC will be in the gel phase at room temperature and hence will give slower permeation rates than unsaturated bilayers, formed from, for example, soy or egg phosphatidylcholine (PC), which exist in the fluid phase. Figure 7 (b) shows how *P* changes with *K*, and also compares the permeation coefficients in this study to earlier values.

The data presented here lie within the range of values reported previously, although there is considerable variation in the values of previous studies. As discussed above, the composition of a bilayer will influence its phase at room temperature, affecting molecular transport rates. Moreover, for membranes formed from soy or egg PC lipids, the paintbrush method has commonly been used to form bilayers, leaving residual organic solvent molecules within the bilayers which may significantly impact on the rate of transport. This may explain the rather weak relationship between *P* and *K* seen in our earlier study[1]; data in Figure 7 (b).

The DPPC data obtained in the present study also show a strong linear trend between *P* and *K* with the exception of acetic acid, where the *P* value is lower than would be expected based on Overton's rule. This observation could be attributed to the gel phase structure of the bilayer creating a greater energy barrier for the permeation of the more hydrophilic molecule, compared to those with longer acyl tails.[50] Li and co-workers, avoided this issue by using a mixture of lipids to ensure the bilayers were in the fluid phase and which explains their higher reported permeation coefficients.[16] The data obtained on fluid phase (soy PC) bilayers herein, show a clear correlation between *P* and *K*, and are in excellent agreement with values reported by Li *et al.* The similarity of our reported permeation coefficients and those determined previously for both gel phase and fluid phase lipids

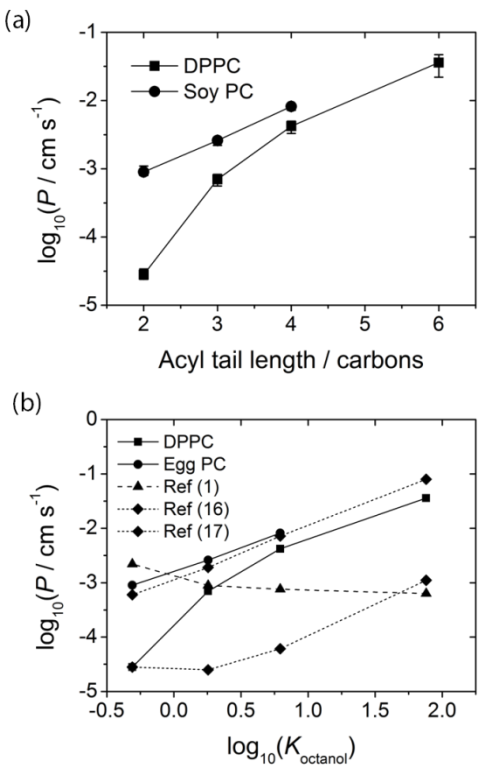

Figure 7. Plots of the permeation coefficient (*P*) of each weak acid across DPPC and soy PC bilayers vs. (a) acyl tail length and

(b) water/octanol partition coefficient (K). In (b) data are also shown for three previous studies.

confirms the validity of our new method of bilayer formation. In particular, the close match between the permeation coefficients determined with soy PC bilayers and those reported for unilamellar vesicles[16] confirms our assumption that this method produces uniform, solvent-free bilayers.

5.4 Effect of Potential Field on Permeability

The configuration developed herein is particularly attractive for allowing the ready study of electric field effects on the rate of transport of molecules across membranes. Potential fields have been shown to increase the rate of transport of ions across lipid membranes via the formation of pores within the membrane,[51, 52] however, there is much less information on the effect of an applied electric field on molecular transport. It is reasonable to postulate that such electric-field induced pores could provide an additional route for the permeation of molecules. Figure 8(a) shows CLSM pH profiles of 5 mM hexanoic acid permeating across bilayers with applied potentials of 0 V, 0.5 V and 1 V. It can be seen visually that there is a clear increase in permeability with increasing potential difference, supporting the idea that the potential field enhances membrane transport. Analysis of these profiles gave permeation coefficients of 6.5×10^{-3} cm s^{-1} at 0 V, 8.1×10^{-3} cm s^{-1} at 0.5 V and 13×10^{-3} cm s^{-1} at 1 V, showing a two-fold increase in permeability from 0 to 1 V. This increase in permeability is unlikely to be due to an increased flux of protons through the pores formed, since the concentration of protons compared to the weak acid differs by over 3 orders of magnitude, indicating that the permeation coefficient of protons would have to be unfeasibly high to account for the change in pH on the trans side of the bilayer.[53]

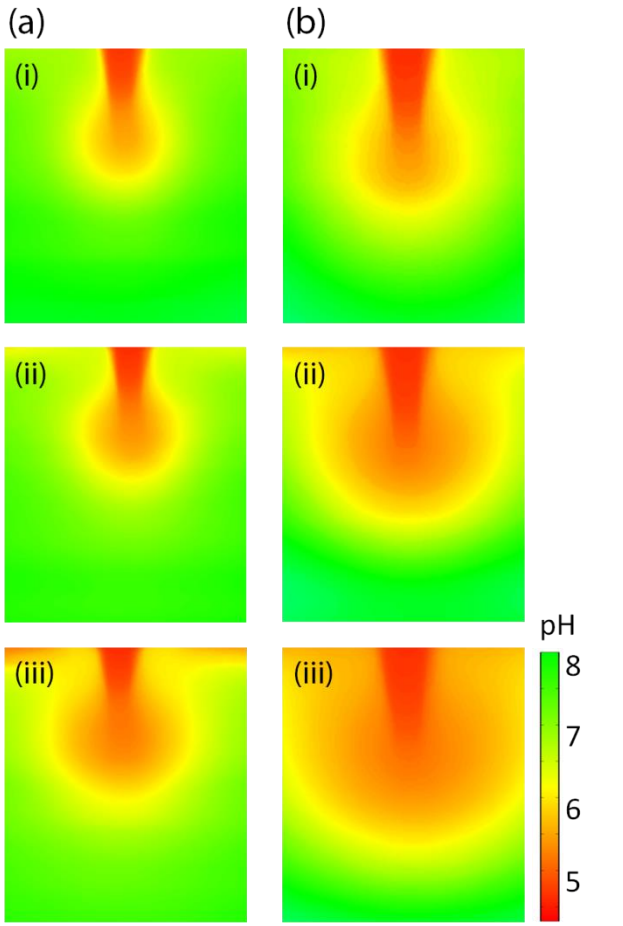

Figure 8. CLSM pH profiles illustrating the permeation of (a) 5 mM hexanoic acid at trans-membrane potentials of (i) 0 V, (ii) 0.5 V and (iii) 1 V and (b) 100 mM propanoic acid at potentials of (i) 0.1 V, (ii) 0.5 V and (iii) 1 V.

The experiment was repeated with propanoic acid, yielding P values of 1.9×10^{-4} cm s^{-1} at 0.1 V, 2.3×10^{-4} cm s^{-1} at 0.5 V, and 3.1×10^{-4} cm s^{-1} at 1 V (Figure 8), indicating that the effect of the potential field on permeability is not influenced by the lipophilicity of the molecule.

Conclusions

A new method of producing suspended BLMs containing negligible amounts of residual solvent molecules at the end of a tapered glass theta pipet has been described. The BLMs can be formed simply and rapidly, are durable over long time periods, and exhibit high seal resistances. This method can be readily coupled with microscopy techniques, such as CLSM used herein, to study the permeation of molecules across these bilayers. The permeation of a series of carboxylic acids across DPPC and soy PC bilayers has been investigated, by monitoring the change in fluorescence intensity of a pH-sensitive fluorophore, allowing the local pH change to be visualized as the weak acid permeated the bilayer. A clear trend was observed from the fluorescence images, with the more lipophilic acids showing larger changes in pH and therefore faster permeation rates. Accurate values for

permeation coefficients have been extracted by fitting experimental data to simulated fluorescence profiles generated by a FEM model that is highly representative of the experimental geometry, so that the permeation coefficient is the only adjustable parameter. Analysis of the fluorescence profiles generated by each carboxylic acid demonstrated that the permeation coefficient is related to the partition coefficient, although the relationship does not strictly follow Overton's rule. This trend applied to both DPPC and soy PC bilayers, however, much higher permeation coefficients were observed for bilayers formed from lipids in the fluid phase (soy PC). An attractive feature of the experimental configuration is that electric field effects on permeation rates can readily be investigated. There is a clear impact of an applied electric field enhancing transport, which we attribute to the formation of pores in the membrane induced by the potential field.

Since weak acids and bases are commonly used as pharmaceutical agents, the technique developed is of considerable value in analyzing permeation rates of these molecules to determine how particular molecular characteristics influence rates of transport. Additionally, there are further possible applications of this technique to asymmetric bilayer studies, due to the method used to form bilayers, via the coupling of individual monolayers. These BLMs could also be investigated as a platform for ion-channel measurements due to their high seal resistances. Indeed, the ability to control the size of the pipet tip opening could allow the system to be optimized for single ion-channel recordings for possible applications as biosensors, where nanometer sized apertures are highly beneficial.[29, 54]

Abbreviations

FEM: finite element method, BLM: bilayer lipid membrane, CLSM: confocal laser scanning microscopy, QRCE: quasi-reference counter electrode, DPPC: 1,2-dipalmitoyl-*sn*-glycero-3-phosphocholine, PC: phosphatidylcholine, USL: unstirred layer

Acknowledgements

K.E.M. thanks the EPSRC Doctoral Training Fund for support (Molecular Organization and Assembly in Cells). B.P.N thanks the University of Warwick (Chancellor's Scholarship) for funding.We acknowledge support from a European Research Council Advanced Investigator Grant (ERC-2009-AdG247143 QUANTIF). Some of the equipment used was obtained through the Science City Advanced Materials project with support from Advantage West Midlands and the European Regional Development Fund. We thank Drs. Kim McKelvey and Alex Colburn for helpful discussions and instrumentation development.

Notes and references

[a] *Department of Chemistry, University of Warwick, Coventry, CV4 7AL (UK). E-mail: p.r.unwin@warwick.ac.uk*
[b] *MOAC Doctoral Training Centre, University of Warwick, Coventry, CV4 7AL (UK)*

† Electronic Supplementary Information (ESI) available: See DOI: 10.1039/b000000x/

1. J. M. A. Grime, M. A. Edwards, N. C. Rudd and P. R. Unwin, *Proc. Natl. Acad. Sci.*, 2008, **105**, 14277-14282.
2. J. M. Wolosin and H. Ginsburg, *Biochim. Biophys. Acta*, 1975, **389**, 20-33.
3. A. Walter, D. Hastings and J. Gutknecht, *J. Gen. Physiol.*, 1982, **79**, 917-933.
4. A. Walter and J. Gutknecht, *J. Membr. Biol.*, 1984, **77**, 255-264.
5. A. Walter and J. Gutknecht, *J. Membr. Biol.*, 1986, **90**, 207-217.
6. V. Y. Evtodienko, O. N. Kovbasnjuk, Y. N. Antonenko and L. S. Yaguzhinsky, *Biochim. Biophys. Acta*, 1996, **1281**, 245-251.
7. E. Orbach and A. Finkelstein, *J. Gen. Physiol.*, 1980, **75**, 427-436.
8. A. Missner, P. Kügler, S. M. Saparov, K. Sommer, J. C. Mathai, M. L. Zeidel and P. Pohl, *J. Biol. Chem.*, 2008, **283**, 25340-25347.
9. M. Kansy, F. Senner and K. Gubernator, *J. Med. Chem.*, 1998, **41**, 1007-1010.
10. K. Sugano, Y. Nabuchi, M. Machida and Y. Aso, *Int. J. Pharm.*, 2003, **257**, 245-251.
11. X. Chen, A. Murawski, K. Patel, C. Crespi and P. Balimane, *Pharm. Res.*, 2008, **25**, 1511-1520.
12. H. Yamada, H. Shiku, T. Matsue and I. Uchida, *The Journal of Physical Chemistry*, 1993, **97**, 9547-9549.
13. M. Tsionsky, J. Zhou, S. Amemiya, F.-R. F. Fan, A. J. Bard and R. A. W. Dryfe, *Anal. Chem.*, 1999, **71**, 4300-4305.
14. C. Overton, *Vierteljahrsschr. Naturforsch. Ges. Zurich.*, 1899, **44**, 88-135.
15. C. Overton, *Studies in Narcosis*, Chapman and Hall, 1901.
16. S. Li, Peichi C. Hu and N. Malmstadt, *Biophys. J.*, 2011, **101**, 700-708.
17. T.-X. Xiang and B. D. Anderson, *Biophys. J.*, 1998, **75**, 2658-2671.
18. H. T. Tien, *Bilayer Lipid Membranes (BLM): Theory and Practice*, Dekker, New York, 1974.
19. P. Mueller, D. O. Rudin, H. T. Tien and W. C. Wescott, *J. Phys. Chem.*, 1963, **67**, 534-535.
20. A. Moscho, O. Orwar, D. T. Chiu, B. P. Modi and R. N. Zare, *Proc. Natl. Acad. Sci.*, 1996, **93**, 11443-11447.
21. M. Montal and P. Mueller, *Proc. Natl. Acad. Sci.*, 1972, **69**, 3561-3566.
22. R. Coronado and R. Latorre, *Biophys J*, 1983, **43**, 231-236.
23. T. Ide and T. Ichikawa, *Biosens. Bioelectron.*, 2005, **21**, 672-677.
24. N. Malmstadt, T. J. Jeon and J. J. Schmidt, *Adv. Mater.*, 2008, **20**, 84-89.
25. X. Lu, A. Leitmannova Ottova and H. T. Tien, *Bioelectrochem. Bioenerg.*, 1996, **39**, 285-289.
26. J. A. Beddow, I. R. Peterson, J. Heptinstall and D. J. Walton, *Anal. Chem.*, 2004, **76**, 2261-2265.
27. M. Hirano, T. Kobayashi and T. Ide, *e-J. Surf. Sci. Nanotech.*, 2008, **6**, 130-133.
28. J. W. Shim and L. Q. Gu, *Anal. Chem.*, 2007, **79**, 2207-2213.
29. R. J. White, E. N. Ervin, T. Yang, X. Chen, S. Daniel, P. S. Cremer and H. S. White, *J. Am. Chem. Soc.*, 2007, **129**, 11766-11775.
30. A. E. P. Schibel, T. Edwards, R. Kawano, W. Lan and H. S. White, *Anal. Chem.*, 2010, **82**, 7259-7266.

31. H. T. Tien and A. Ottova-Leitmannova, *Membrane Biophysics*, Elsevier, Amsterdam, The Netherlands, 2000.
32. S. Li, P. Hu and N. Malmstadt, *Anal. Chem.*, 2010, **82**, 7766-7771.
33. B. A. Suarezisla, K. Wan, J. Lindstrom and M. Montal, *Biochem.*, 1983, **22**, 2319-2323.
34. A. Hirano, M. Wakabayashi, Y. Matsuno and M. Sugawara, *Biosens. Bioelectron.*, 2003, **18**, 973-983.
35. D. Marsh, *Biochimica et Biophysica Acta (BBA) - Reviews on Biomembranes*, 1996, **1286**, 183-223.
36. S. M. Saparov, Y. N. Antonenko and P. Pohl, *Biophys. J.*, 2006, **90**, L86-L88.
37. C. Davies, *Ion Association*, Butterworths, London, 1962.
38. A. E. P. Schibel, E. C. Heider, J. M. Harris and H. S. White, *J. Am. Chem. Soc.*, 2011, **133**, 7810-7815.
39. N. Fertig, C. Meyer, R. H. Blick, C. Trautmann and J. C. Behrends, *Phys. Rev. E*, 2001, **64**, 040901.
40. O. S. Andersen, *Biophys. J.*, 1983, **41**, 119-133.
41. Q. Li, S. Xie, Z. Liang, X. Meng, S. Liu, H. H. Girault and Y. Shao, *Angew. Chem. Int. Ed.*, 2009, **48**, 8010-8013.
42. A. Bruckbauer, D. Zhou, L. Ying, Y. E. Korchev, C. Abell and D. Klenerman, *J. Am. Chem. Soc.*, 2003, **125**, 9834-9839.
43. G. Taylor and H. H. J. Girault, *J. Electroanal. Chem.*, 1986, **208**, 179-183.
44. C. G. Williams, M. A. Edwards, A. L. Colley, J. V. Macpherson and P. R. Unwin, *Anal. Chem.*, 2009, **81**, 2486-2495.
45. M. E. Snowden, A. G. Güell, S. C. S. Lai, K. McKelvey, N. Ebejer, M. A. O'Connell, A. W. Colburn and P. R. Unwin, *Anal. Chem.*, 2012, **84**, 2483-2491.
46. P. H. Barry and J. M. Diamond, *Physiol. Rev.*, 1984, **64**, 763-872.
47. T. Korjamo, A. T. Heikkinen and J. Mönkkönen, *J. Pharm. Sci.*, 2009, **98**, 4469-4479.
48. Y. N. Antonenko, G. A. Denisov and P. Pohl, *Biophys. J.*, 1993, **64**, 1701-1710.
49. N. C. Rudd, S. Cannan, E. Bitziou, I. Ciani, A. L. Whitworth and P. R. Unwin, *Anal. Chem.*, 2005, **77**, 6205-6217.
50. T. X. Xiang and B. D. Anderson, *Biophys. J.*, 1997, **72**, 223-237.
51. J. C. Weaver and Y. A. Chizmadzhev, *Bioelectrochem. Bioenerg.*, 1996, **41**, 135-160.
52. K. Kinosita, I. Ashikawa, N. Saita, H. Yoshimura, H. Itoh, K. Nagayama and A. Ikegami, *Biophys. J.*, 1988, **53**, 1015-1019.
53. D. W. Deamer, *J. Bioenerg. Biomembr.*, 1987, **19**, 457-479.
54. H. Bayley and P. S. Cremer, *Nature*, 2001, **413**, 226-230.